CHEMISTRY
A EUROPEAN JOURNAL

DOI: 10.1002/chem.200800262

Selective C–C Coupling of Ir–Ethene and Ir–Carbenoid Radicals

Wojciech I. Dzik, Joost N. H. Reek, and Bas de Bruin*[a]

Abstract: The reactivity of the paramagnetic iridium(II) complex $[Ir^{II}(ethene)(Me_3tpa)]^{2+}$ (**1**) (Me_3tpa = *N*,*N*,*N*-tris(6-methyl-2-pyridylmethyl) amine) towards the diazo compounds ethyl diazoacetate (EDA) and trimethylsilyldiazomethane (TMSDM) was investigated. The reaction with EDA gave rise to selective C–C bond formation, most likely through radical coupling of the Ir–carbenoid radical species $[Ir^{III}\{CH^{\bullet}(COOEt)\}(MeCN)(Me_3tpa)]^{2+}$ (**7**) and (the MeCN adduct of) **1**, to give the tetracationic dinuclear complex $[(MeCN)(Me_3tpa)Ir^{III}\{CH(COOEt)CH_2CH_2\}Ir^{III}(MeCN)(Me_3tpa)]^{2+}$ (**4**). The analogous reaction with TMSDM leads to the mononuclear dicationic species $[Ir^{III}\{CH_2(SiMe_3)\}(MeCN)(Me_3tpa)]^{2+}$ (**11**). This reaction probably involves a hydrogen-atom abstraction from TMSDM by the intermediate Ir–carbenoid radical species $[Ir^{III}\{CH^{\bullet}(SiMe_3)\}(MeCN)(Me_3tpa)]^{2+}$ (**10**). DFT calculations support pathways proceeding via these Ir–carbenoid radicals. The carbenoid–radical species are actually carbon-centered ligand radicals, with an electronic structure best described as one-electron-reduced Fischer-type carbenes. To our knowledge, this paper represents the first reactivity study of a mononuclear Ir^{II} species towards diazo compounds.

Keywords: carbenes · iridium · radicals · redox chemistry

Introduction

Our understanding of the organometallic reactivity of rhodium and iridium is primarily based on studies of diamagnetic complexes. Much less is known about the reactivity of their paramagnetic analogues.[1] In general, open-shell organometallic species reveal rather different reactivity patterns with respect to their closed-shell counterparts, broadening the scope of organometallic chemistry for catalytic processes, which explains the rapidly growing interest in such compounds.[2] A number of such interesting reactions, unique to those of paramagnetic organometallic complexes or intermediates, have already been uncovered. One-electron oxidative addition of organic halides to the metal is a key step in Ru-catalyzed atom-transfer radical polymerization[3] and in Ru-,[4] and Rh/Ir-catalyzed[4d] atom-transfer radical addition of polyhalogenated compounds to olefins. In addition, Rh^{II}–porphyrin complexes are capable of homolytic cleavage of inert C–H bonds of methane[5] or methanol[6] and cleave the C–C bonds of ketones,[7] nitriles,[8] and the 2,2,6,6-tetramethylpiperidine-*N*-oxide radical (TEMPO).[9] A recent study by Chan describes the selective formation of $[Rh^{III}(CH_2COOEt)(por)]$ (por = tmp = tetramesityl porphyrin) upon reaction of $[Rh^{II}(por)]$ with ethyl diazoacetate (EDA),[10] likely via an open-shell carbenoid species, which is relevant to the work described in this paper.

Bergman reported enantioselective carbene transfer from diazo compounds to olefins and imines mediated by $[Rh^{II}(benbox)Cl]^{+}$ (benbox = benzyl bis(oxazoline)), thus presenting a rare example of a catalytically active paramagnetic mononuclear Rh^{II} complex.[11] Although a variety of Group 9 complexes are capable of carbene-transfer catalysis,[12] this area of research is clearly dominated by investigations of diamagnetic Doyle-type dinuclear, acetate-bridged, Rh^{II}–Rh^{II} species (and analogues) and a couple of mononuclear diamagnetic M^{III} catalysts.[12,13] Remarkably, the reactivity of both mononuclear (diamagnetic) M^{I} and mononuclear (paramagnetic) M^{II} complexes (M = Rh, Ir) towards diazo compounds has received almost no attention. We previously set out to investigate the reactivity of M^{I} complexes towards diazo compounds, which led to our recent discovery that mononuclear M^{I}–diene complexes (M = Rh, Ir) mediate the formation of polymers from ethyl diazoacetate.[14] Motivated by these initial results, we became interested in the influence of the oxidation state on the reactivity of mononu-

[a] W. I. Dzik, Prof. Dr. J. N. H. Reek, Dr. B. de Bruin
Department of Homogeneous and Supramolecular Catalysis
Van't Hoff Institute for Molecular Sciences (HIMS)
University of Amsterdam, Nieuwe Achtergracht 166
1018 WV Amsterdam (The Netherlands)
Fax: (+31) 20-525-6422
E-mail: bdebruin@science.uva.nl

Supporting information for this article is available on the WWW under http://www.chemeurj.org/ or from the author.

clear Rh– and Ir–carbene complexes. Further inspired by our general interest in the reactivity of paramagnetic Rh^{II} and Ir^{II} species, we now report on the reactivity of a mononuclear Ir^{II}–ethene complex towards ethyl diazoacetate and trimethylsilyldiazomethane, which are common carbene precursors.

Results and Discussion

We concentrated on the reactivity of our previously reported paramagnetic Ir^{II}–ethene complex $[Ir^{II}(ethene)(Me_3tpa)]^{2+}$ (**1**) ($Me_3tpa = N,N,N$-tris(6-methyl-2-pyridylmethyl)amine). Interestingly, complex **1** reveals both "metalloradical" and "alkene radical" behavior (Scheme 1).[1a,b,15]

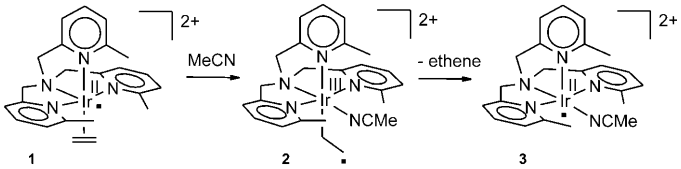

Scheme 1. Reactivity of $[Ir^{II}(ethene)(Me_3tpa)]^{2+}$ towards MeCN.

The "vacant" site *cis* to the ethene ligand is sterically shielded by the three methyl groups of the Me_3tpa ligand, and therefore not accessible for larger molecules. However, the small and linear MeCN can bind to this position, by which it induces ethene-ligand-centered radical reactivity. We previously proposed that β-ethyl radicals of the type $[Ir^{III}(CH_2CH_2)^{\bullet}(Me_3tpa)]^{2+}$ (**2**) could be intermediates in a series of radical-type reactions triggered by coordination of MeCN to the otherwise stable metalloradical **1**.[15] Ethene loss from intermediate **2** should be easy, giving access to the metalloradical $[Ir^{II}(MeCN)(Me_3tpa)]^{2+}$ (**3**). Somewhat similar behavior of $[Ir^{II}(por)]$ species in their reactivity towards ethene has been reported.[16]

Hence, we were not sure what to expect for the reactivity of complex **1** towards diazo compounds. Would they react directly with **1**, or would such reaction preferably take place via **2** or **3** in the presence of MeCN? One-electron activation of diazo compounds may allow radical-type reactions of its "carbene" moiety. Such reactivity might be useful for expanding carbon chains of olefins.

The reaction of complex **1** towards ethyl diazoacetate (EDA) in acetone leads to a complex mixture of compounds. In contrast, the reaction of **1** with EDA in MeCN proceeds selectively as judged from the ^1H NMR spectrum. The reaction results in formation of the tetracationic dinuclear C_3-bridged species $[(Me_3tpa)(MeCN)Ir^{III}\{CH_2CH_2CH(COOEt)\}Ir^{III}(MeCN)(Me_3tpa)]^{4+}$ (**4**) in 74% isolated yield, see Scheme 2.

Addition of excess EDA does not have any influence on the outcome of the reaction. The reactivity of **1** with EDA in MeCN could reflect the metalloradical behavior of **3**, the ethene-ligand–radical behavior of **2**, or both. In absence of

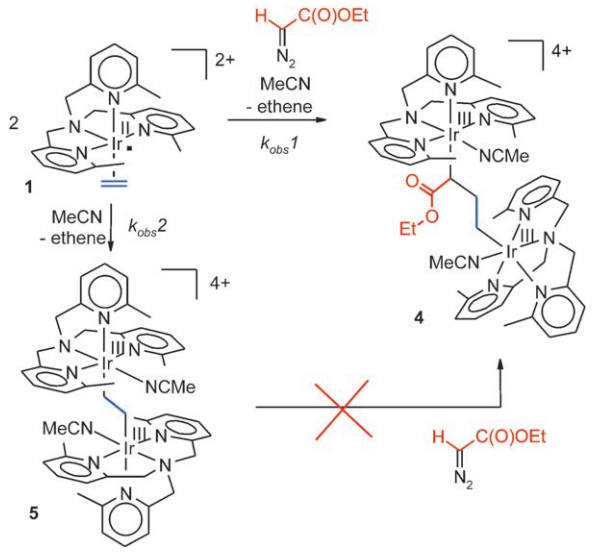

Scheme 2. Reaction of **1** with EDA in MeCN to give **4**. In absence of EDA compound **1** converts to **5**. The observed rate constants for the two reactions are identical ($k_{obs}1 = k_{obs}2$).

EDA, **1** in MeCN slowly converts to the ethylene-bridged dinuclear iridium complex $[(Me_3tpa)(MeCN)Ir^{III}(\mu_2\text{-}CH_2CH_2)Ir^{III}(MeCN)(Me_3tpa)]^{4+}$ (**5**).[15a] Complex **5**, however, does not react with EDA, so carbene insertion (from EDA) into the Ir–C bond of **5** to form **4** can be excluded as a mechanistic pathway.

Two mechanistic pathways seem conceivable: A) Dissociation of ethene from **1** with formation of **3**, followed by coordination of the diazo compound to iridium (to give **6**) with subsequent loss of dinitrogen to form the "carbenoid–radical" **7**, which in turn attacks the ethene fragment of **1** or **2** to form the new C–C bond of **4**; or B) attack of the ethene carbon-centered radical of **2** at the diazo carbon atom of EDA to form the γ-alkyl radical $Ir^{III}\text{–}CH_2CH_2CH^{\bullet}(COOEt)$ species **9**, which would eventually couple with the Ir-centered radical **3**. These routes are depicted in Scheme 3.

EPR measurements did not allow us to detect any intermediates during the conversion of **1** to **4**; even in the presence of a large excess of EDA only gradually disappearing signals of **1** were detected. Also the reaction kinetics did not allow us to discriminate between the reaction pathways A and B in Scheme 3. The kinetic measurements revealed that the reaction is first-order in [**1**] and zero-order in [EDA], and proceeds at exactly the same rate as observed for the formation of **5** in absence of EDA ($k_{obs}1 = k_{obs}2 = 0.0075\ min^{-1}$). So ethene dissociation from **2**, or MeCN coordination to **1** are the most likely rate limiting steps (Scheme 3, formation of **2** or **3**).

In absence of more experimental details we resorted to DFT calculations to obtain more information about the possible reaction mechanisms leading to **4**. We used methyl diazoacetate to model EDA. Given the importance of the three methyl fragments on the reactivity of $[Ir^{II}(ethene)(Me_3tpa)]^{2+}$, we decided to model the complete dications.

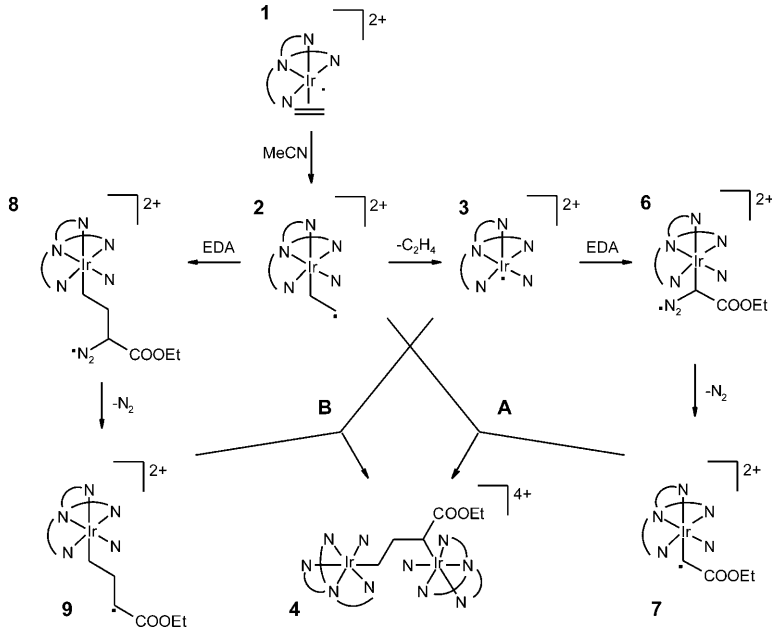

Scheme 3. Conceivable pathways to the C_3-bridged bis-iridium species **4**.

Due to the substantial size of the full Ir–Me_3tpa system, we did not try to calculate the transition states or energies associated with the final radical couplings in Scheme 2 (**3**+**9**→**4** or **2**+**7**→**4**). Besides, this would not be very useful, because DFT energies of reactions that involve spin-state changes, such as radical–radical coupling reactions, are generally not very reliable.[9a,17] The reaction pathways prior to the actual coupling, however, all deal with $S=1/2$ systems, and the relative energies of the minima and transition states along the pathways **1**→**2**→**8**→**9** and **1**→**2**→**3**→**6**→**7** should be meaningful.

Both reaction pathways (A and B in Scheme 3) are thermodynamically favorable, with an overall stair-case decrease of free energies along the reaction coordinates (Scheme 4).

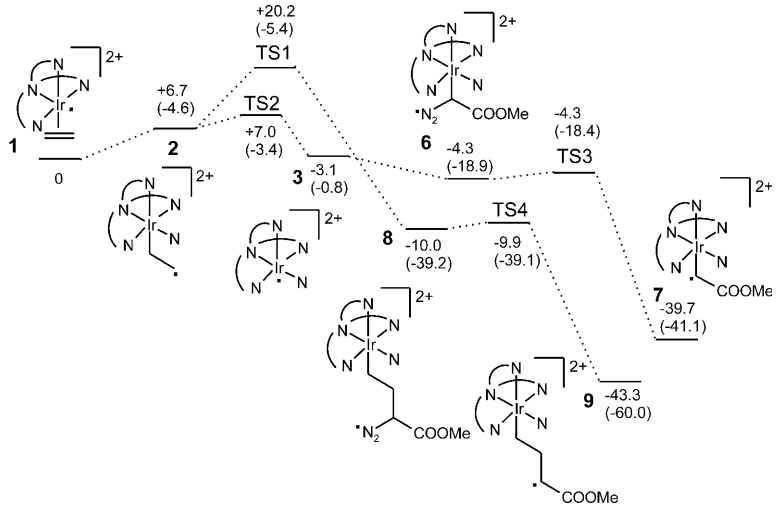

Scheme 4. Calculated free energies (energies) in kcal mol^{-1} of the intermediates and transition states in routes A and B leading to formation of **4** (see also Scheme 3).

Formation of **2** from **1** is slightly uphill, but this is mainly due to (gas-phase) entropy effects associated with the approach of MeCN, which do not play a large role in the experimental system in which MeCN is used as a solvent.

The transition state (TS) for ethene loss from **2** (**TS2**) represents a very low barrier ($\Delta G_{\mathbf{2}\rightarrow\mathbf{TS2}}=+0.3$ kcal mol^{-1}) for formation of **3**. This barrier is most likely too low, as DFT tends to underestimate the iridium–ethene interactions.[18] This becomes evident, and worse, upon using the hybrid HF-DFT functional b3-lyp, at which level (TZVP basis) species **2** proved unstable and converged to **3** by spontaneous ethene dissociation.[19] For reasons of comparison, we thus used the BP86 (SV(P) basis) throughout. Although the actual barrier for ethene loss from **2** might be somewhat higher than calculated, it is unlikely to be very high. Therefore the involvement of species **2** can only be relevant for low-barrier follow-up reactions. This is not the case in the reaction of **2** with MDA to form **8**, which has a relatively large barrier (**TS1**, $\Delta G_{\mathbf{2}\rightarrow\mathbf{TS1}}=+13.5$ kcal mol^{-1}). In contrast, the approach of MDA to bind to the Ir center of **3** (reaction **3**→**6**) has a very flat energy profile and is essentially barrierless (see Supporting Information, Figure S11). Thus MDA binding to the β-carbon atom of **2** seems unlikely, since pathway A is kinetically preferred over pathway B according to the DFT calculations.

Once formed, the MDA adducts **6** and **8** both reveal a remarkably low barrier for N_2 loss (**TS4** ≈0.1 kcal mol^{-1}, **TS3** is essentially barrierless once entropy corrections are applied). This is in marked contrast with substantially higher calculated barriers (in the range of 7–12 kcal mol^{-1}) for N_2 loss from MDA and diazoalkane adducts of closed-shell Rh^I species.[14a,20]

We argued that we might obtain additional experimental evidence for the reaction proceeding by pathway A by using a bulkier substituted diazo compound. Sufficient steric bulk should prevent the organo-

metalic radicals from coupling, and if the reaction would proceed through pathway A, the expected final product would be a mononuclear iridium compound derived from a bulky analogue of **7**. In fact, trimethylsilyldiazomethane (TMSDM) proved to be a proper reagent for checking this hypothesis.

The reaction of **1** with TMSDM in MeCN affords the mononuclear iridium compound **11** in 41% isolated yield. Compound **11** has a methylene(trimethylsilyl) group bound to the metal (Scheme 5). This is consistent with the above

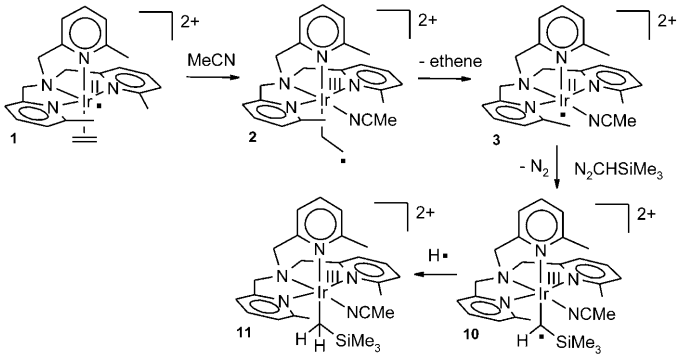

Scheme 5. Formation of iridium (trimethylsilyl)methylene **11** consistent with a carbenoid–radical pathway.

DFT calculations predicting the "carbenoid–radical" pathway (A) to be kinetically preferred over a direct C–C coupling between the diazo carbon atom and the β-carbon of ethyl–radical complex **2**.

The "carbenoid–radical" intermediate **10** abstracts a hydrogen atom from the reaction medium. The solvent is not the source of the hydrogen atom, as experiments in deuterated solvents did not lead to incorporation of deuterium. The most likely source is the (trimethylsilyl)diazomethane reagent.[10]

The key reactive species responsible for the formation of **4** and **11** thus seem to be the carbenoid–radical species **7** and **10**, respectively. Such [Ir^{II}(carbene)(N-ligand)] complexes cannot be classified as regular Fischer- or Schrock-type carbenes, and their unusual electronic structure (Scheme 6) requires some additional comments. As shown in Figure 1 for complex **7**, the species are primarily carbon-centered radicals. Most of the spin density of **7** is located at its carbenoid carbon atom (Mulliken spin densities: $C_{carbene}$: 86%, Ir: 5%, $O_{carbonyl}$: 12%, $C_{carbonyl}$: −4%, O_{Me}: 5%, $H_{carbene}$: −5%).

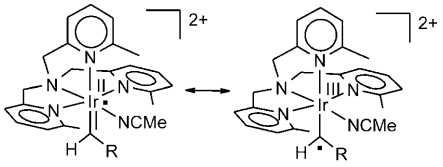

Scheme 6. "Redox non-innocence" of open-shell transition-metal carbene complexes; The Ir^{II}–carbene complexes **7** and **10** are best described as Ir^{III}–carbon-centered radicals.

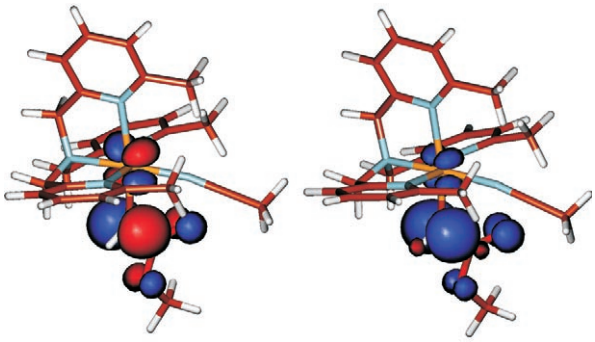

Figure 1. SOMO (left) and spin density (right) plots of **7**.

The SOMO of **7** is primarily built from the carbenoid carbon p orbital in antibonding combination with an Ir d orbital with a smaller orbital coefficient (d_{xz} if we define the z axis along the Ir–C bond and the x axis along the Ir–N_{amine} bond), with some expected delocalization over the adjacent carbonyl fragment (Figure 1). The carbenoid–radical **7** is thus best described as a one-electron-reduced Fischer-type carbene complex (Figure 2, top).[22] In good agreement with

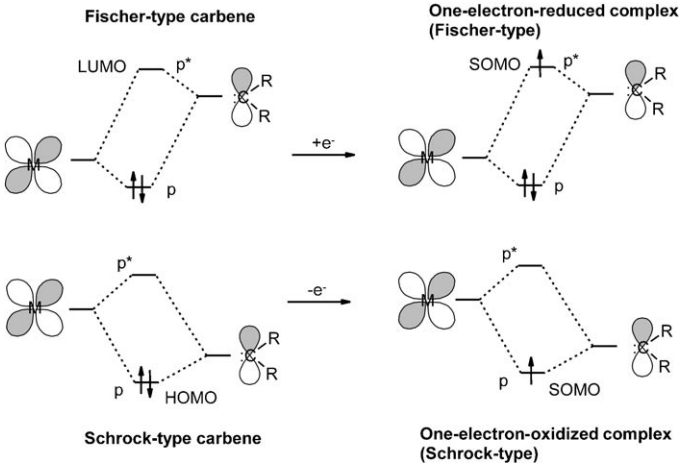

Figure 2. Schematic representation of the frontier orbitals involved in formation of carbon-centered radicals by one-electron reduction of Fischer-type carbenes (top) or one-electron oxidation of Schrock-type carbenes (bottom).

occupation of an electron in the Ir–C antibonding orbital (π*), which reduces the Ir–C bond order, the calculated Ir–C bond of **7** (2.02 Å) is comparably long compared to related closed-shell systems (≈1.85–1.91 Å).[14a,20] A schematic representation of the calculated d-orbital configuration of all five 5d orbitals is presented in the Supporting Information (Figure S12).

It is quite remarkable that the redox chemistry of transition-metal carbene complexes has thus far received so little attention. The frontier orbitals of both Fischer- and Schrock-type carbenes are such that the carbene fragment

must be "redox non-innocent" (Scheme 6). In a Fischer-type carbene, the carbene-carbon p orbital lies higher in energy than the transition-metal d orbital with which it interacts through π-bonding. This leads to a primarily carbon-centered LUMO, giving the carbene fragment its intrinsic electrophilic character. Apparently this orbital arrangement also allows the formation of a carbon-centered radical upon one-electron reduction of a Fischer-type carbene, as in case of **7** and **10** (See Figure 1). The carbon p orbital of a Schrock-type carbene lies lower in energy than the transition-metal d orbital with which it interacts leading to a primarily carbon-centered HOMO. This gives the carbene fragment its intrinsic nucleophilic character and should allow the formation of a carbon-centered radical upon one-electron oxidation (we are not aware of any such reported examples yet), see Figure 2.

Thus obtained carbon-centered radicals can not be described as regular Fischer- or Schrock-type carbenes, and actually represent a new class of "one-electron-activated carbenoids". For Group 9 elements (Co, Rh, Ir), we are aware of only one such previously claimed example.[21] More general, reactivity studies of open-shell carbenoid complexes (one-electron-activated carbene complexes) are in an early stage of development and only a few reports describe the formation of C–C bonds through open-shell carbenoid–radical complexes.[22] The redox non-innocence of more stable *N*-heterocyclic carbenes was addressed very recently.[23]

Conclusion

We demonstrated the unprecedented formation of a paramagnetic iridium bound "carbenoid–radical" complex that selectively couples to an Ir^{II}–ethene species with formation of a C–C bond. A more bulky "carbenoid–radical", obtained by reacting trimethylsilyl diazomethane with the Ir^{II}–ethene complex, abstracts a hydrogen atom from the reaction medium instead of undergoing C–C coupling with an Ir^{II}–ethene species. DFT calculations show that the unpaired electron density of both "carbenoid–radical" species resides mainly on the "carbenoid" carbon atom, explaining the reactivity of the two complexes. This study expands the scope of known reactivity of diazo compounds and allows the consideration of "carbenoid radical" species in selective C–C bond formation reactions. Further studies aiming at revealing further details of the remarkable reactivity of similar carbenoid radicals of Rh and Ir are underway.

Experimental Section

General procedures: All manipulations were performed in an argon atmosphere by standard Schlenk techniques or in a glove box. Acetonitrile was distilled under argon from CaH_2. NMR experiments were carried out on a Bruker DRX300 (300 and 75 MHz for ^1H and ^{13}C respectively) and Varian Inova (500 MHz for ^1H). Solvent shift reference: [D_3]acetonitrile $\delta = 1.94$ and 1.24 ppm for ^1H and ^{13}C, respectively. Abbreviations used are s = singlet, d = doublet, t = triplet, m = multiplet. Elemental analysis (CHN) was carried out by H. Kolbe Mikroanalytisches Laboratorium (Germany). Kinetic measurements were performed on Perkin–Elmer Lambda 5 UV/Vis spectrometer in a thermostated quartz Schlenk cuvette at 20 °C. X-band EPR spectroscopy measurements were performed with a Bruker EMX Plus spectrometer. Fast atom bombardment (FAB) mass spectrometry was carried out on a JEOL JMS SX/SX 102 A four-sector mass spectrometer, coupled to a JEOL MS-MP9021D/UPD system program. Samples were loaded in a matrix solution (3-nitrobenzyl alcohol) on to a stainless steel probe and bombarded with Xenon atoms with an energy of 3 KeV. During the high-resolution FAB-MS measurements a resolving power of 10000 (10% valley definition) was used.

Ethyl diazoacetate and a 2 M solution of (trimethylsilyl)diazomethane in diethyl ether were obtained from Aldrich, and used without further purification. Complex **1** ([Ir^{II}(ethene)(Me_3tpa)][PF_6]$_2$) was prepared as described before.[15a]

Synthesis of [(Me_3tpa)(MeCN)Ir($CH_2CH_2CHCOOEt$)Ir(MeCN)(Me_3tpa)][PF_6]$_4$ (4): Compound **1** (48 mg, 0.057 mmol) was dissolved in MeCN (4 mL). Subsequently EDA (6 μL, 0.057 mmol) was added by using a micropipette and the reaction was stirred overnight. The reaction mixture was concentrated to approximately 0.5 mL and MeOH (4 mL) was added causing precipitation of **4** as a white powder. Yield: 38 mg (0.021 mmol, 74%). ^1H NMR (500 MHz, CD_3CN): $\delta = 7.99$ (t, $^3J(H,H) = 7.5$ Hz, 1H), 7.90 (m, 2H), 7.82 (t, $^3J(H,H) = 7.5$ Hz, 1H), 7.65 (2H, m), 7.53 (d, $^3J(H,H) = 7.5$ Hz, 1H), 7.42 (d, $^3J(H,H) = 7.5$ Hz, 2H), 7.34 (m, 4H), 7.25 (d, $^3J(H,H) = 8$ Hz, 1H), 7.21 (d, $^3J(H,H) = 7.5$ Hz, 2H), 7.16 (d, $^3J(H,H) = 7.5$ Hz, 1H), 7.13 (d, $^3J(H,H) = 7.5$ Hz, 1H), 5.45 (d, $^2J(H,H) = 16$ Hz, 1H), 5.38 (d, $^2J(H,H) = 15.5$ Hz, 1H), 5.24 (d, $^2J(H,H) = 16.5$ Hz, 1H), 4.88 (d, $^2J(H,H) = 17.5$ Hz, 1H), 4.85 (d, $^2J(H,H) = 17$ Hz, 2H), 4.76–4.65 (m, 3H), 4.59 (s, 2H), 4.48 (d, $^2J(H,H) = 16$ Hz, 1H), 3.79 (m, 1H; -OCH_2CH$_3$), 3.63 (d, $^3J(H,H) = 11.5$ Hz, 1H; Ir-CH-COOEt), 3.10 (s, 6H; PyCH$_3$), 2.923 (s, 3H; Ir-NCCH$_3$), 2.917 (s, 3H; Ir-NCCH$_3$), 2.81 (m, 1H; -OCH_2CH$_3$), 2.79 (s, 3H; PyCH$_3$), 2.65 (s, 3H; PyCH$_3$), 2.60 (s, 3H; PyCH$_3$), 2.32 (s, 3H; PyCH$_3$), 2.29 (m, 2H; Ir-CH$_2$), 1.05 (m, 1H; CH$_2$CH_2CHCOOEt), 0.67 (t, ^{3}J(H,H)7 Hz, 3H; OCH$_2$CH_3), −0.28 ppm (m, 1H; CH$_2$CH_2CHCOOEt); ^{13}C NMR (75 MHz, CD_3CN): $\delta = 182.8$ (COOEt), 165.9, 165.5, 165.2, 164.9, 164.8, 164.4, 164.0, 163.8, 163.4, 162.6, 159.1, 158.2 (Py-C$^{2/6}$), 141.7, 141.4, 141.2, 140.6, 140.2 (Py-C^4), 129.2, 128.8, 128.7, 128.6, 128.4, 127.7, 123.2, 122.7, 122.6, 122.2, 120.3, 120.1 (Py-C$^{3/5}$), 74.7, 74.2, 71.1, 71.03, 70.96, 70.6 (Py-CH$_2$-N), 60.6 (OCH$_2$CH$_3$), 33.5 (C-CH2-C), 27.5, 27.30, 27.25, 27.1, 26.6 (Py-CH$_3$), 13.9 (OCH$_2$CH$_3$), 11.1 (Ir-CH(COOEt)), −2.0 ppm (Ir-CH$_2$); elemental analysis calcd (%) for $C_{52}H_{64}F_{24}Ir_2N_{10}O_2P_4$: C 34.21, H 3.53, N 7.67; found: C 34.50, H 3.64, N 7.32.

Synthesis of [Ir{$CH_2Si(CH_3)_3$}(MeCN)(Me_3tpa)][PF_6]$_2$ (11): Compound **1** (57 mg, 0.068 mmol) was dissolved in MeCN (4 mL). Subsequently, a 2 M solution of (trimethylsilyl)diazomethane in Et_2O (34 μL, 0.068 mmol) was added by using a micropipette and the reaction was stirred overnight. The reaction mixture was concentrated to approximately 0.5 mL and CH_2Cl_2 (4 mL) was added, causing a little precipitation of **5**. The solution was decanted and the solvent was removed under vacuum to afford brown solid. The solid was redissolved in MeCN, and EtOH was added causing precipitation of a brown oil which was discarded. Decanting and removing the solvent under vacuum yielded **11** as an off-white powder. Yield: 26 mg (0.028 mmol, 41%); ^1H NMR (300 MHz, CD_3CN): $\delta = 7.82$ (t, $^3J(H,H) = 7.5$ Hz, 2H; Py^A-H^4), 7.65 (t, $^3J(H,H) = 7.8$ Hz, 1H; Py^B-H4), 7.38–7.29 (m, 5H; Py^A-H^3, Py^A-H^5, PyB), 7.15 (d, $^3J(H,H) = 7.5$ Hz, 1H; Py^B), 5.26 (d[AB], $^2J(H,H) = 16.2$ Hz, 2H; N-CH$_2$-Py^A), 4.83 (d[AB], $^2J(H,H) = 16.2$ Hz, 2H; N-CH$_2$-Py^A), 4.63 (s, 2H; N-CH$_2$-Py^B), 3.14 (s, 3H; Py^B-CH$_3$), 2.91 (s, 3H; IrNC-CH$_3$), 2.81 (s, 6H; Py^A-CH$_3$), 1.50 (s, 2H; Ir-CH$_2$-Si), −0.27 ppm (s, 9H; Si-CH$_3$); ^{13}C NMR (75 MHz, CD_3CN): $\delta = 165.7$ (Py^A-C^6), 164.8 (Py^A-C^2), 162.8 (Py^B-C^6), 158.9 (Py^B-C^2), 140.8 (Py^A-C^4), 140.1 (Py^B-C^4), 128.5 (Py^A), 127.9 (Py^B), 122.5 (Py^A), 120.2 (Py^B), 74.4 (Py^B-CH$_2$-N), 71.3 (Py^A-CH$_2$-N), 27.2 (Py^A-CH$_3$), 27.0 (Py^B-CH$_3$), 5.8 (IrNCCH3), −20.3 ppm (Ir-CH$_2$-Si); the IrNCCH$_3$ and Si-CH$_3$ signals were obscured by the solvent signal; FAB$^+$-MS: *m*/*z*: 798.2 [M−PF_6]$^+$, 672.3 [M−2PF_6+F]$^+$, 631.2 [M−2PF_6+F−MeCN)]$^+$.

DFT calculations: The geometry optimizations were carried out with the Turbomole program[24] coupled to the PQS Baker optimizer.[25] Geometries were fully optimized as minima or transition states at the BP86[26] level using the SV(P) basis set[27] on all atoms (small-core pseudopotential[28] on iridium). All stationary points were characterized by vibrational analysis (numerical frequencies); ZPE and thermal corrections (entropy and enthalpy, 298 K, 1 bar) from these analyses are included. The thus obtained (free) energies (kcal mol^{-1}) are reported in Scheme 3. Optimized geometries of the species **1–9** and **TS 1**–**TS 4** are supplied as pdb files in the Supporting Information. The orbital and spin density plots shown in Figure 1 were generated with Molden.[29]

Acknowledgements

We thank the Netherlands Organization for Scientific Research (NWO-CW) for financial support. We thank Jan Meine Ernsting and Jan Geenevasen for their assistance with the NMR experiments, Han Peeters for measuring FAB$^+$-MS mass spectra, Taasje Mahabiersing for his assistance with the kinetic measurements, and Prof. Dr. Peter H. M. Budzelaar for helpful tips and tricks concerning the DFT calculations.

[1] For reviews about mononuclear Rh^{II} and Ir^{II} species, see: a) D. G. H. Hetterscheid, H. Grützmacher, A. J. J. Koekoek, B. de Bruin, *Prog. Inorg. Chem.* **2007**, *55*, 247–354; b) B. de Bruin, D. G. H. Hetterscheid, *Eur. J. Inorg. Chem.* **2007**, 211–230; c) D. G. DeWit, *Coord. Chem. Rev.* **1996**, *147*, 209–246; d) K. K. Pandey, *Coord. Chem. Rev.* **1992**, *221*, 1–42.

[2] a) D. Astruc, *Electron-Transfer and Radical Processes in Transition-Metal Chemistry*, VCH, Weinheim, **1995**; b) M. C. Baird, *Chem. Rev.* **1988**, *88*, 1217–1227; c) "Organometallic Radical Processes": *J. Organomet. Chem. Libr.* **1990**, *22*, whole volume; d) N. G. Connelly, *Chem. Soc. Rev.* **1989**, *18*, 153–185; e) Paramagnetic Organometallic Species in Activation/Selectivity, Catalysis: *NATO ASI Ser. Ser. C* **1987**, *257*, whole volume; f) L. A. MacAdams, G. P. Buffone, C. D. Incarvito, J. A. Golen, A. L. Rheingold, K. H. Theopold, *Chem. Commun.* **2003**, *10*, 1164–1165; g) C. Pariya, K. H. Theopold, *Curr. Sci.* **2000**, *78*, 1345–1351; h) J. D. Jewson, L. M. Liable-Sands, G. P. A. Yap, A. L. Rheingold, K. H. Theopold, *Organometallics* **1999**, *18*, 300–305; i) R. Poli, *Chem. Rev.* **1996**, *96*, 2135–2204; j) C. Limberg, *Angew. Chem.* **2003**, *115* 6112–6136; *Angew. Chem. Int. Ed.* **2003**, *42*, 5932–5954.

[3] a) H. Takahashi, T. Ando, M. Kamigaito, M. Sawamoto, *Macromolecules* **1999**, *32*, 3820–3823; b) M. Kamigaito, T. Ando, M. Sawamoto, *Chem. Rev.* **2001**, *101*, 3689–3745 (review).

[4] a) H. Matsumoto, T. Nakano, Y. Nagai, *Tetrahedron Lett.* **1973**, *14*, 5147–5150; b) F. Simal, L. Wlodarczak, A. Dimonceau, A. F. Noels, *Tetrahedron Lett.* **2000**, *41*, 6017–6074; c) review: K. Severin, *Curr. Org. Chem.* **2006**, *10*, 217–224; d) A. E. Díaz-Álvarez, P. Crochet, M. Zablocka, C. Duhayon, V. Cadierno, J.-P. Majoral, *Eur. J. Inorg. Chem.* **2008**, *5*, 786–794.

[5] A. E. Sherry, B. B. Wayland, *J. Am. Chem. Soc.* **1990**, *112*, 1259–1261.

[6] W. Cui, X. P. Zhang, B. B. Wayland, *J. Am. Chem. Soc.* **2003**, *125*, 4994–4995.

[7] L. Zhang, K. S. Chan, *J. Organomet. Chem.* **2006**, *691*, 3782–3787.

[8] a) K. S. Chan, X. Z. Li, C. W. Fung, L. Zhang, *Organometallics* **2007**, *26*, 20–21; b) K. S. Chan, X. Z. Li, C. W. Fung, L. Zhang, *Organometallics* **2007**, *26*, 2679–2687.

[9] a) K. S. Chan, X. Z. Li, W. I. Dzik, B. de Bruin, *J. Am. Chem. Soc.* **2008**, *130*, 2051–2061; b) K. W. Mak, S. K. Yeung, K. S. Chan, *Organometallics* **2002**, *21*, 2362–2364; c) M. K. Tse, K. S. Chan, *J. Chem. Soc. Dalton Trans.* **2001**, 510–511.

[10] L. Zhang, K. S. Chan, *Organometallics* **2007**, *26*, 679–684.

[11] J. R. Krumper, M. Gerisch, J. M. Suh, R. G. Bergman, T. D. Tilley, *J. Org. Chem.* **2003**, *68*, 9705–9710.

[12] For examples of Co- and Rh-catalyzed reactions, see: M. P. Doyle, D. C. Forbes, *Chem. Rev.* **1998**, *98*, 911–935, and references therein.

[13] Recently an [Ir^{III}(salen)] complex proved as efficient catalyst for cyclopropanation of styrene: S. Kanchiku, H. Suematsu, K. Matsumoto, T. Uchida, T. Katsuki, *Angew. Chem.* **2007**, *119*, 3963–3965; *Angew. Chem. Int. Ed.* **2007**, *46*, 3889–3891.

[14] a) E. Jellema, P. H. M. Budzelaar, J. N. H. Reek, B. de Bruin, *J. Am. Chem. Soc.* **2007**, *129*, 11631–11641; b) D. G. H. Hetterscheid, C. Hendriksen, W. I. Dzik, J. M. M. Smits, E. R. H. van Eck, A. E. Rowan, V. Busico, M. Vacatello, V. Van Axel Castelli, A. Segre, E. Jellema, T. G. Bloemberg, B. de Bruin, *J. Am. Chem. Soc.* **2006**, *128*, 9746–9752.

[15] a) D. G. H. Hetterscheid, J. Kaiser, E. J. Reijerse, T. P. J. Peters, S. Thewissen, A. N. J. Blok, J. M. M. Smits, R. de Gelder, B. de Bruin, *J. Am. Chem. Soc.* **2005**, *127*, 1895–1905; b) D. G. H. Hetterscheid, M. Bens, B. de Bruin, *Dalton Trans.* **2005**, 979–984.

[16] H. Zhai, A. Bunn, B. B. Wayland, *Chem. Commun.* **2001**, 1294–1295.

[17] Hybrid HF/DFT functionals (such as b3-lyp) tend to overestimate the relative stability of radicals compared to closed-shell systems: a) M. Saeys, M.-F. Reyniers, G. B. Marin, V. Van Speybroeck, Waroquir, *J. Phys. Chem. A* **2003**, *107*, 9147–9159; b) R. Sustmann, W. Sicking, R. Huisgen, *J. Am. Chem. Soc.* **2003**, *125*, 14425–14434; c) K. P. Jensen, U. Ryde, *J. Phys. Chem. A* **2003**, *107*, 7539–7545; d) A. Gosh, *J. Biol. Inorg. Chem.* **2006**, *11*, 712–724.

[18] a) S. Thewissen, Ph.D. Thesis, Radboud University Nijmegen (The Netherlands), **2005**; b) P. H. M. Budzelaar, A. N. J. Blok, *Eur. J. Inorg. Chem.* **2004**, *11*, 2385–2391.

[19] Benchmark studies of 5d transition metals are lacking, but for 3d and 4d transition metals hybrid HF-DFT methods such as b3-lyp or B3LYP tend to underestimate the metal–ligand bond strengths. Deviations from experimental values are generally smaller for pure DFT methods, such as BP86: a) J. N. Harvey, *Annu. Rep. Prog. Chem. Sect. C* **2006**, *102*, 203–226; b) N. E. Schultz, Y. Zhao, D. G. Truhlar, *J. Phys. Chem. A* **2005**, *109*, 11127–11143; c) F. Furche, J. P. Perdew, *J. Chem. Phys.* **2006**, *124*, 044103(1)-044103(27); d) M. P. Waller, H. Braun, N. Hojdis, M. Bühl, *J. Chem. Theory Comput.* **2007**, *3*, 2234–2242; see also references [17c] and [17d].

[20] R. Cohen, B. Rybtchinski, M. Gandelman, H. Rozenberg, J. M. L. Martin, D. Milstein, *J. Am. Chem. Soc.* **2003**, *125*, 6532–6546.

[21] T. Ikeno, I. Iwakura, T. Yamada, *J. Am. Chem. Soc.* **2002**, *124*, 15152–15153.

[22] M. A. Sierra, M. Gómez-Gallego, R. Martínez-Álverez, *Chem. Eur. J.* **2007**, *13*, 736–744, and references therein.

[23] B. Tumanskii, D. Sheberla, G. Molev, Y. Apeloig, *Angew. Chem.* **2007**, *119*, 7552–7555; *Angew. Chem. Int. Ed.* **2007**, *46*, 7408–7411.

[24] a) Turbomole Version 5: R. Ahlrichs, M. Bär; H.-P. Baron, R. Bauernschmitt, S. Böcker, M. Ehrig, K. Eichkorn, S. Elliott; F. Furche, F. Haase, M. Häser, C. Hättig, H. Horn, C. Huber, U. Huniar, M. Kattannek, A. Köhn, C. Kölmel, M. Kollwitz, K. May, C. Ochsenfeld, H. Öhm, A. Schäfer, U. Schneider, O. Treutler, K. Tsereteli, B. Unterreiner, M. von Arnim, F. Weigend, P. Weis, H. Weiss, Theoretical Chemistry Group, University of Karlsruhe, January **2002**; b) O. Treutler, R. Ahlrichs, *J. Chem. Phys.* **1995**, *102*, 346–354.

[25] a) PQS version 2.4, **2001**, Parallel Quantum Solutions, Fayetteville, Arkansas, USA (the Baker optimizer is available separately from PQS upon request); b) J. Baker, *J. Comput. Chem.* **1986**, *7*, 385–395.

[26] a) A. D. Becke, *Phys. Rev. A* **1988**, *38*, 3098–3100; b) J. P. Perdew, *Phys. Rev. B* **1986**, *33*, 8822–8824.

[27] A. Schäfer, H. Horn, R. Ahlrichs, *J. Chem. Phys.* **1992**, *97*, 2571–2577.

[28] a) Turbomole basisset library, Turbomole Version 5, see [24a]. b) D. Andrae, U. Haeussermann, M. Dolg, H. Stoll, H. Preuss, *Theor. Chim. Acta* **1990**, *77*, 123–141.

[29] G. Schaftenaar, J. H. Noordik, *J. Comput.-Aided Mol. Des.* **2000**, *14*, 123–134.

Received: February 12, 2008
Published online: June 3, 2008

